JETP Letters, Vol. 80, No. 5, 2004, pp. 293–297. Translated from Pis'ma v Zhurnal Éksperimental'noĭ i Teoreticheskoĭ Fiziki, Vol. 80, No. 5, 2004, pp. 339–343.

Linear and Nonlinear Optical Spectroscopy of Gadolinium Iron Borate $GdFe_3(BO_3)_4$

A. M. Kalashnikova[1, *], V. V. Pavlov[1], R. V. Pisarev[1], L. N. Bezmaternykh[2], M. Bayer[3], and Th. Rasing[4]

[1] *Ioffe Physicotechnical Institute, Russian Academy of Sciences, St. Petersburg, 194021 Russia*
**e-mail: kalashnikova@mail.ioffe.ru*
[2] *Institute of Physics, Siberian Division, Russian Academy of Sciences, Krasnoyarsk, 660036 Russia*
[3] *Experimental Physics II, Dortmund University, Dortmund, 44227 Germany*
[4] *NSRIM Institute, University of Nijmegen, 6525 the Netherlands*

Received July 20, 2004

The optical spectra and the second-harmonic generation (SHG) are studied in a noncentrosymmetric $GdFe_3(BO_3)_4$ magnet. In the region of weak absorption ($\alpha \sim 20$–400 cm^{-1}) below ~3 eV, three absorption bands are distinguished, which can be unambiguously assigned to forbidden electronic transitions from the ground $^6A_1$ state of the Fe^{3+} ion to its excited states $^4T_1$ (~1.4 eV), $^4T_2$ (~2 eV), and $^4A_1$, ^4E (~2.8 eV). Intense absorption begins in the region above 3 eV ($\alpha \sim 2$–4×10^5 cm^{-1}), where two bands at ~4.0 and 4.8 eV are observed, which are caused by allowed electric dipole charge-transfer transitions. The spectral features of SHG in the 1.2–3.0-eV region are explained by a change in the SHG efficiency caused by a change in the phase mismatch. It is shown that in the weak absorption region, phase matching can be achieved for SHG. © *2004 MAIK "Nauka/Interperiodica".*

PACS numbers: 42.65.Ky; 71.20.Eh; 78.20.Ci; 78.20.Hp

Substances and structures in which several subsystems with different order parameters can be distinguished have attracted attention since the 1960s and are called multiferroics [1–4]. These parameters can be spontaneous magnetization and antiferromagnetic vector in magnets, spontaneous electric polarization in ferroelectrics, spontaneous deformation in ferroelastics, etc. In multiferroics, interaction between subsystems is possible when certain spatial and temporal symmetry conditions are fulfilled. Cross-interactions in multiferroics open up new possibilities for the development of devices based on the mutual control of magnetic, electric, and deformation states. Initial attempts to develop competitive devices proved to be unsuccessful due to the weakness of the interactions observed. However, quite recently several studies were reported that demonstrated a revival of interest in multiferroics. Materials and multiphase heterostructures with "giant" effects were synthesized [5–10], which opens up the outlook for applications of multiferroics in information systems as sensors and in spintronic devices.

Rare-earth iron borates with the general formula $RFe_3(BO_3)_4$, where R is a rare-earth element, are characterized by an unusual combination of a number of physical properties and can be assigned, according to some of these properties, to multiferroics. They are crystallized into the trigonal huntite structure described by the noncentrosymmetric space group R32 (no. 155) with three formula units in the unit cell, $Z = 3$ [11]. Note that crystals with the huntite structure have the same point group 32, as crystalline quartz but, of course, differ from quartz in their chemical composition and, hence, in their physical properties. A change in temperature induces structural and magnetic phase transitions in iron borates, but their character is not clear at present in most cases [11–14]. Magnetic ordering can, in principle, occur both in the iron and rare-earth sublattices, and these sublattices also determine the optical properties of rare-earth iron borates.

Trivalent Fe^{3+} ions in the $RFe_3(BO_3)_4$ crystal structure occupy the 9*d* octahedral sites with the local symmetry *2*, which form one-dimensional (1D) helicoid chains extended along the trigonal axis [11]. The octahedral sites of the Fe^{3+} ion are typical of many other oxide iron compounds including, for example, centrosymmetric iron borate $FeBO_3$, rare-earth orthoferrites $RFeO_3$, and ferrite garnets $R_3Fe_5O_{12}$. However, a significant difference between the crystalline structures of huntite and these materials, and especially the noncentrosymmetric arrangement of magnetic ion sites and the noncentrosymmetric structure of huntite itself should result in a number of substantial differences between the optical properties of rare-earth iron borates and the oxides of trivalent iron studied earlier. Note that, in the huntite structure, as in quartz, the second-harmonic generation (SHG) is allowed in the electric dipole approximation [15]. For the point group 32, the $yyy = -xxy = -xyx = -yxx$, $xyz = -yzx$, and $xzy = -yzx$

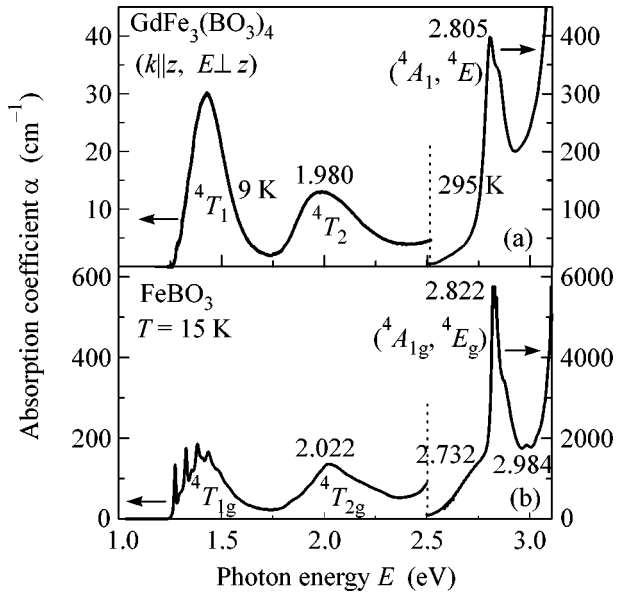

Fig. 1. Absorption spectra of (a) gadolinium iron borate $GdFe_3(BO_3)_4$ at T = 9 and 295 K and (b) iron borate $FeBO_3$ at T = 15 K.

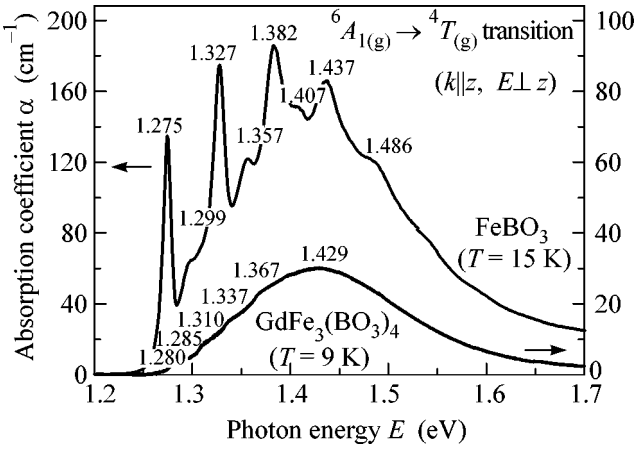

Fig. 2. Absorption spectra of $GdFe_3(BO_3)_4$ and $FeBO_3$ at the ${}^6A_1({}^4A_{1g}) \longrightarrow {}^4T_1({}^4T_{1g})$ transition.

components of the susceptibility $\chi_{ijk}(2\omega)$ of the second harmonic are nonzero [3].

In this paper, we report a comparative study of optical absorption, birefringence, and SHG in gadolinium iron borate $GdFe_3(BO_3)_4$. We also present the results of the ellipsometric study of this material in the region between 0.6 and 5.4 eV, performed in the reflection geometry. This allowed us to determine the dispersion of the main optical parameters in a broad spectral range. The results obtained suggest that it is possible to produce phase matching for SHG in this magnetic material, which, as far as we know, was not investigated earlier for other magnetic materials [16].

The $GdFe_3(BO_3)_4$ single crystals were grown by the method described in [13]. Optical studies were performed with plane-parallel oriented plates of thickness from 0.1 to 1.0 mm. The absorption spectra were recorded using a Cary 2300 spectrophotometer and a Spex monochromator. The SHG spectra were studied in the transmission geometry at the normal incidence of the fundamental radiation on a sample. The method described in [17] was used. The ellipsometric study was performed using an ellipsometer at several angles of the incidence of light on a sample, which allowed us to determine with good accuracy the ordinary and extraordinary refractive indices n_o and n_e, the absorption coefficients k_o and k_e, and the birefringence $\Delta n = n_o - n_e$.

The linear absorption spectra of gadolinium iron borate and iron borate are shown in Fig. 1. They are qualitatively similar on the whole. Absorption in the region below 3.0 eV is comparatively weak, and it was studied in the transmission geometry along the optical axis. In this region three absorption bands are observed, which correspond to the electronic transitions between the $(3d)^5$ states of the shell of the Fe^{3+} ion in the octahedral crystal field produced by oxygen O^{2-} ions [18]. Because the transitions from the ${}^6A_1$ ground state to the excited ${}^4T_1$ and ${}^4T_2$ states and the degenerate $({}^4A_1, {}^4E)$ state are forbidden by the spin-selection rules, the intensity of the corresponding absorption bands is comparatively low. Moreover, the intensity of these transitions in $GdFe_3(BO_3)_4$ is substantially lower than in $FeBO_3$ and other trivalent iron oxides. Figure 2 shows the absorption spectra in the region of the first ${}^6A_1 \longrightarrow {}^4T_1$ transition for gadolinium iron borate and $FeBO_3$. The Fe^{3+} ion in both these materials is located in the octahedral environment consisting of six O^{2-} ions, which produce a crystal field and cause the splitting of the degenerate states of a free ion. In our case, this is the ${}^4G$ state [18]. The Fe–O bond lengths in these compounds are close and are 2.028 Å in $FeBO_3$ [19] and 2.026(2) Å, 2.044(2) Å, and 1.950(2) Å (the average bond length is 2.007 Å) in $GdFe_3(BO_3)_4$ [11]. The values of the parameter $10Dq$ of the cubic crystal field are also close, as was confirmed by the coincidence of the positions of the absorption bands of these compounds with an accuracy of 1–2%. Two observations are surprising: (i) the absence of the fine structure in the region of the first transition in gadolinium iron borate. We cannot yet explain this unexpected fact; and (ii) a substantial decrease in the intensity of absorption bands in gadolinium iron borate by approximately a factor of six for the first transition, by a factor of ten for the second transition, and by a factor of fifteen for the third transition, although, unlike $FeBO_3$, the Fe^{3+} ion in this iron borate is located in the noncentrosymmetric environment. The difference between the absorption-band intensities increases in the approach to the fundamental absorption edge determined by the allowed transitions. Even more illustrative is a comparison of iron borates with orthof-

errites $RFeO_3$, in which the Fe–O bonds vary from 2.006 to 2.014 Å [20]. According to our measurements, the maximum absorption coefficient for the first transition in orthoferrites is $\alpha \simeq 400$ cm^{-1}.

One can see from Fig. 3b that absorption above 3.0 eV is stronger, and it should be assigned to the allowed electric dipole transitions. In oxides of 3*d* transition metals, these are charge-transfer transitions [21]. In the cluster model, this is the electron transfer from the oxygen ion to the iron ion, while in the band model, this is an electronic transition from the valence band formed predominantly by the oxygen 2*p* orbitals to the conduction band formed predominantly by the 3*d* orbitals. One can see from Fig. 3a that the observed transitions are polarized, resulting in the crystallographic birefringence $\Delta n = n_o - n_e$ and in linear dichroism $\Delta k = k_o - k_e$. In the relatively transparent region, $\Delta k \simeq 0$ and $\Delta n \simeq 0.1$; i.e., birefringence is rather strong, and the crystal is negative. Note for comparison that birefringence in crystal quartz in the visible region has the opposite sign and is on the order of $\Delta n \sim 0.06$–0.07 [22]; i.e., it is somewhat lower than in gadolinium iron borate.

In the region of intense absorption, two absorption bands are observed at ~4.0 and 4.8 eV. Let us compare these spectra with the spectra of other iron oxides. The intense absorption bands of $FeBO_3$ lie in the region from 3.38 to 3.75 eV [23], while in orthoferrites such bands are located, according to our data, at even lower energies, namely, 3.16, 3.9, and 4.4 eV. This redshift of the allowed electric dipole transitions qualitatively explains the increase in the intensity of the forbidden *d*–*d* transition in passing from gadolinium iron borate to $FeBO_3$ and orthoferrites, because forbidden transitions borrow the intensity of allowed transitions; the smaller their separation, the greater the degree of borrowing. Therefore, although the Fe–O bond lengths are almost the same in different materials and, hence, the local crystal fields are close, the optical properties of these materials can be substantially different. A significant difference between the spectra of iron borates and orthoferrites is already manifested in the fact that the former are transparent at a sample thickness of a few hundred micrometers in the green spectral region at 2.4 eV (see Fig. 1), while the latter are transparent only at thicknesses on the order of a hundred micrometers in the red spectral region at 2.0 eV [24]. In both cases, the absorption bands are caused by the transitions in the 3*d* shell of the Fe^{3+} ion in the region below ~3.0 eV and by the charge-transfer transitions at ~3.0 eV. In our opinion, the great difference in the absorption spectra of iron borates and orthoferrites is mainly explained by the difference in their crystal structures. The Fe–O–Fe bonds in orthoferrites form a three-dimensional network, whereas this bond in gadolinium iron borate, is in fact, one-dimensional and is realized only along the octahedral chains extended along the trigonal axis while the chains are not coupled to each other [11].

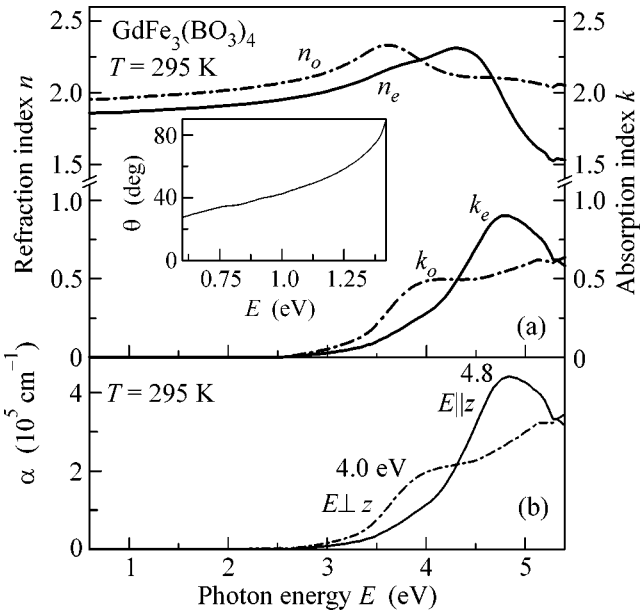

Fig. 3. (a) Dispersion of the ordinary (dot-and-dash curve) and extraordinary (solid curve) refractive indices and absorption coefficients of $GdFe_3(BO_3)_4$ at $T = 295$ K. Inset: dependence of the phase-matching angle θ on the pump energy. (b) Absorption spectra for light propagating along (dot-and-dash curve) and perpendicular to (solid curve) the optical axis.

It is known that most magnetic materials are centrosymmetric media, and SHG is forbidden in the electric dipole approximation. Nevertheless, SHG can be observed in magnetic materials with various centrosymmetric and noncentrosymmetric structures due to the break of the inversion center caused by magnetic ordering or the inclusion of magnetic dipole transitions into the three-photon process of harmonic generation [16]. Iron borates crystallize into the R32 noncentrosymmetric structure, and hence, SHG is allowed in the electric dipole approximation. We studied SHG in the transmission geometry, in which light propagated along the optical axis $\mathbf{k} \parallel z$ in a sample of thickness $t = 100$ μm. Figure 4 shows the SHG intensity $I_{2\omega}$ normalized to the squared fundamental radiation intensity I_ω^2. The inset in Fig. 4 shows the azimuthal dependence of the SHG intensity $I_{2\omega} \sim (\chi_{xxx} \cos 3\varphi)^2$, where φ is the angle between the crystal axes in the basal plane of a trigonal crystal and the polarization vector of the fundamental light wave. The results were obtained in the region of comparatively weak absorption. The SHG signal drastically decreases when absorption increases to $\alpha \simeq 400$ cm^{-1} at the $^6A_1 \longrightarrow (^4A_1, {}^4E)$ transition (see Fig. 1) and then vanishes as absorption further increases in the region above ~3.0 eV.

The decrease in the SHG signal with increasing absorption is also explained by a change in the coherence length, which is predominantly determined in the

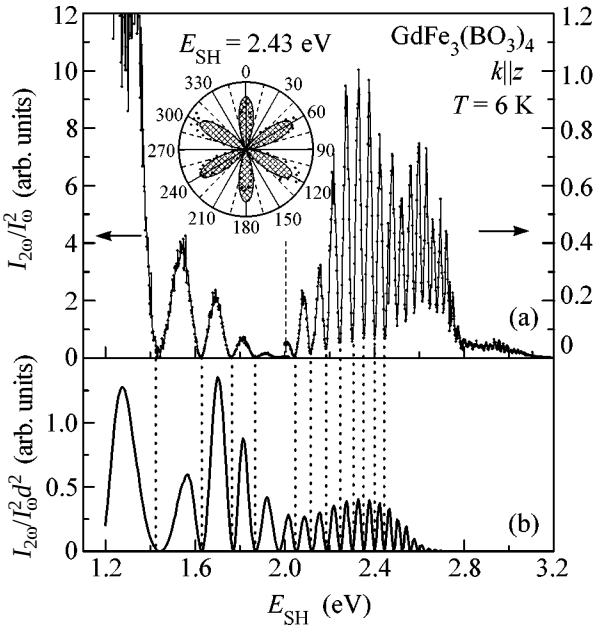

Fig. 4. (a) Spectral dependence of SHG in $GdFe_3(BO_3)_4$ at T = 6 K. Inset: azimuthal dependence of the SHG signal for the energy E_{SH} = 2.43 eV. (b) Spectral dependence of the SHG intensity calculated by expression (1).

transparency region by the dispersion of the refractive index and gradually decreases from ~15 to 0.9 μm in the region from 0.6 to 1.6 eV (from 1.2 to 3.2 eV for the second harmonic).

The oscillatory spectral dependence of the SHG intensity can be explained by the mechanism of Maker fringes observed upon changing the angle of incidence of fundamental radiation on a crystal [25, 26]. In our case, oscillations are caused by a change in the SHG efficiency that is not due to a change in the effective path length of light in the crystal but due rather to a change in the phase mismatch $\Delta\kappa = 2\kappa_\omega - \kappa_{2\omega}$ when the fundamental frequency varied, where $\kappa = n_\omega\omega/c$ is the wavenumber at the corresponding frequency. In this case, the dependence of the SHG intensity on the light frequency is described by the expression [15]

$$I_{2\omega} \sim \frac{d^2 I_\omega^2(2\omega)^2}{n_\omega^2 n_{2\omega}} L^2 \frac{\sin^2(\Delta\kappa L/2)}{(\Delta\kappa L/2)^2}, \qquad (1)$$

where $d_{ijk} = \frac{1}{2}\chi_{ijk}^{(2\omega)}$, and L is the crystal thickness. The function $I_{2\omega}/I_\omega^2 d^2$ calculated by expression (1) is presented in Fig. 4b. We also took into account in the calculation the absorption of the SHG signal. One can see from this figure that the periodicities of the experimental and calculated spectra coincide.

Figure 3a shows that $GdFe_3(BO_3)_4$ crystals have large birefringence $\Delta n \simeq 0.1$, allowing the realization of phase matching of the first type (*ooe*) in $GdFe_3(BO_3)_4$ for the efficient SHG. The inset in Fig. 3 presents the dependence of the phase-matching angle on the pump energy. In particular, the phase-matching angle for a pump energy of 1.17 eV from a Nd:YAG laser is $\theta \simeq 52°$. In our opinion, the above conclusion about the possibility of realizing phase matching in the magnetic material permits the extension of studies of the relation between the magnetic and nonlinear optical properties.

We thank H.-J. Weber and O. Schöps for their help in measuring the absorption spectra. This work was supported in part by the Russian Foundation for Basic Research, Deutsche Forschungsgemeinschaft, and the European program "Dynamics."

REFERENCES

1. *Magnetoelectric Interaction Phenomena in Crystals*, Ed. by A. J. Freeman and H. Schmid (Gordon and Breach, London, 1975).
2. G. A. Smolenskiĭ and I. E. Chupis, Usp. Fiz. Nauk **137**, 415 (1982) [Sov. Phys. Usp. **25**, 475 (1982)].
3. R. R. Birss, *Symmetry and Magnetism* (North-Holland, Amsterdam, 2000).
4. H. Schmid, *Magnetoelectric Effects in Insulating Magnetic Materials*, reprinted from *Introduction to Complex Mediums for Optics and Electromagnetics*, Ed. by W. S. Weigloger and A. Lakhtakia (SPIE Press, Bellingham, WA, 2003).
5. M. Fiebig, C. Degenhardt, and R. V. Pisarev, Phys. Rev. Lett. **88**, 027203 (2002).
6. T. Kimura, T. Goto, H. Shintani, *et al.*, Nature **429**, 392 (2004).
7. J. Wang, J. B. Neaton, H. Zheng, *et al.*, Science **299**, 1719 (2003).
8. Th. Lottermoser, Th. Lonkai, U. Amman, *et al.*, Nature **430**, 541 (2004).
9. G. Srinivasan, E. T. Rasmussen, B. J. Levin, and R. Hayes, Phys. Rev. B **65**, 134402 (2002).
10. C. W. Nan, L. Lin, N. Cai, *et al.*, Appl. Phys. Lett. **81**, 3831 (2002).
11. J. A. Campá, C. Cascales, E. Guitiérres-Puebla, *et al.*, Chem. Mater. **9**, 237 (1997).
12. Y. Hinatsu, Y. Doi, K. Ito, *et al.*, J. Solid State Chem. **172**, 438 (2003).
13. A. D. Balaev, L. N. Bezmaternykh, I. A. Gudim, *et al.*, J. Magn. Magn. Mater. **258–259**, 532 (2003).
14. R. Z. Levitin, E. A. Popova, R. M. Chtsherbov, *et al.*, Pis'ma Zh. Éksp. Teor. Fiz. **79**, 531 (2004) [JETP Lett. **79**, 423 (2004)].
15. R. W. Boyd, *Nonlinear Optics* (Academic, San Diego, 1992).
16. M. Fiebig, V. V. Pavlov, and R. V. Pisarev, J. Opt. Soc. Am. B (in press).
17. M. Fiebig, D. Fröhlich, St. Leute, and R. V. Pisarev, Appl. Phys. B **66**, 265 (1998).

18. A. B. P. Lever, *Inorganic Electronic Spectoscopy*, 2nd ed. (Elsevier, Amsterdam, 1984).
19. *Landolt–Börnstein, Numerical Data and Functional Relationships in Science and Technology* (Springer, Berlin, 1993), Group III, Vol. 27h.
20. M. Marezio, J. P. Remeika, and P. D. Derneir, Acta Crystallogr. B **26**, 2008 (1970).
21. A. I. Likhtenshteĭn, A. S. Moskvin, and V. A. Gubanov, Fiz. Tverd. Tela (Leningrad) **24**, 3596 (1982) [Sov. Phys. Solid State **24**, 2049 (1982)].
22. *Handbook on Physical Constants*, Ed. by I. S. Grigoriev and E. Z. Meĭlikhov (Énergoatomizdat, Moscow, 1991; CRC, Boca Raton, 1997).
23. A. V. Malakhovskii and I. S. Edelman, Phys. Status Solidi B **74**, K145 (1976).
24. F. J. Kahn, P. S. Pershan, and J. P. Remeika, Phys. Rev. **186**, 891 (1969).
25. P. D. Maker, R. W. Terhune, M. Nisenoff, and C. M. Savage, Phys. Rev. Lett. **8**, 21 (1962).
26. J. Jerphagnon and S. K. Kurtz, J. Appl. Phys. **41**, 1667 (1970).

Translated by M. Sapozhnikov